International Journal of Engineering Trends and Technology
ISSN: 2231–5381 / https://doi.org/10.14445/22315381/IJETT-V73I8P114

Volume 73 Issue 8, 170-179, August 2025


*Original Article*

# Experimental Investigation of Underwater Erosion Abrasion Resistance of Geopolymer and Conventional Mortar Using ASTM C1138 Test Method

Arief Subakti Ariyanto[1,3]*, Slamet Imam Wahyudi[2], Muhammad Mukhlisin[3]

[1,2]*Civil Engineering Department, Sultan Agung Islamic University, Semarang, Indonesia.*
[3]*Jurusan Teknik Sipil Politeknik Negeri Semarang, Indonesia.*

[1]*Corresponding Author : arief.subakti@polines.ac.id*

Received: 27 February 2025 Revised: 19 July 2025 Accepted: 31 July 2025 Published: 30 August 2025

***Abstract -*** *Damage to hydraulic structures' surfaces, spillways, bridge pillars, and channel walls occurs due to surface friction between particles carried in the water, like sand, gravel, and debris flow. This surface abrasion damage will affect the operational lifespan. For this reason, materials that have qualified abrasion resistance are needed. Geopolymers are one of the materials that can be used. Geopolymer is an environmentally friendly material with aluminosilicate and alkali activator as the base material. This study's novelty is using geopolymer materials as a binder for mortars. In this study, the geopolymer was made with a one-component system, stirred dryly with a ratio of binder and aggregate of 1:2, and the geopolymer design was made with 14 Molar. Abrasion testing is carried out using the ASTM C 1138 Underwater test method. From the test, the results of the abrasion test of geopolymer mortar at the age of 28 days were 1.318 8 x $10^{-4}$ $m^3$ with a compressive strength of 47.61 MPa, while normal mortar with a composition of 1:2 was 1.45 x $10^{-5}$ $m^3$ and a compressive strength of 28.45 MPa.*

***Keywords -*** *Abrasion, Hydraulic surface, Geopolymer, ASTM C 1138, Compressive strength.*

## 1. Introduction

Hydraulic structures such as bridge piers, dams, spillways, canals, and stilling basins are frequently subjected to high-velocity water flows laden with sediment. A primary concern is the progressive deterioration of concrete surfaces due to prolonged exposure to sediment-laden flows, which significantly reduces the expected service life of these structures. [1,2]. A comprehensive understanding of the mechanisms contributing to concrete surface degradation is critical for the effective design and rehabilitation of hydraulic structures. Surface damage is governed by multiple factors, including the particle dimensions and loading of suspended sediments, the hydraulic velocity of sediment-bearing flow, the impact angle of the hydraulic stream, the duration of exposure, and the intrinsic quality of the concrete material [3, 4]. According to ACI 207.6R-17 [5].

Surface deterioration of masonry and concrete in hydraulic structures primarily results from erosion mechanisms such as cavitation, abrasion, and chemical degradation. Cavitation and abrasion are categorized as physical processes, while chemical degradation arises from reactions between concrete constituents and aggressive chemical agents transported by water. Cavitation damage typically manifests as localized pitting or voids, in contrast to abrasion, which produces smoother, worn surfaces. The most severe abrasion effects are attributed to suspended solid particles such as sand, gravel, silt, ice, and other debris that continuously impact and scour the hydraulic surface throughout the operational lifespan of the hydraulic structure [6].

The influence of abrasion damage plays a vital role in maintaining a structure's service life. Good planning and material selection are required because abrasive damage is inevitable and impossible to avoid. Figure 1 shows the Abrasion damage and the damage process.

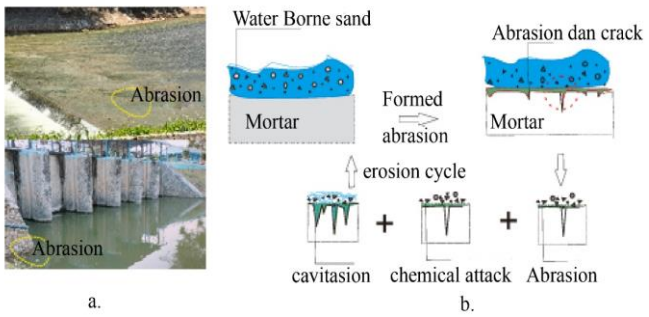


**Fig. 1(a) Surface degradation, and (b) The process of damage to the surface of the hydraulic structure. (source: author documentation)**

Abrasion and erosion are long-term damage processes that do not appear at the beginning of the water building structure's operation. After the operation, damage due to abrasion and erosion will appear, affecting the water building structure. Generally, abrasion and erosion damage occur in overflow basins, carrier channels, tunnels, and waterways [7].

To maintain the hydraulic structure to remain reliable and increase the structure's service life, the concrete must resist abrasion damage. The materials that make up the concrete and rubble stone masonry consist of a binder and an aggregate. So far, the use of binders with Portland cement bases has increased by 2.5% per year, with 3500 billion tons in 2020 and 4400 billion tons in 2030 [8]. The use of OPC globally ranks second after water as the most used material [9, 10]. OPC is a material that requires much energy in the production process, after steel and aluminum. The OPC production process produces $CO_2$. The production of Ordinary Portland Cement (OPC) results in $CO_2$ emissions comprising approximately 325 kg per ton from fuel combustion, 525 kg per ton from the calcination of limestone, and an additional 50 kg per ton associated with electricity consumption. Consequently, manufacturing one ton of OPC releases an estimated 0.8 to 1 ton of $CO_2$ to the atmosphere [11].

In response to this challenge, various studies have explored alternative binders, particularly geopolymers and alkali-activated materials, due to their lower carbon footprint and enhanced durability characteristics [12]. These binders, made from industrial byproducts like fly ash, ceramics waste, and glass waste, offer a sustainable and durable alternative for hydraulic use. Geopolymers show promising chemical resistance and low porosity, aiding abrasion resistance [13].

## 2. Research Significant

This research has significant value because it aims to fill the research gap in developing binder materials that are environmentally friendly and have high abrasion resistance, especially for applications in hydraulic structures. In addition, this study also proposes a new analytical approach to quantitatively measure surface abrasion by utilizing artificial intelligence through OpenCV-based image processing techniques.

## 3. Materials and Methods

### *3.1. Material*

*3.1.1. Ordinary Portland Cement (OPC)*

The OPC utilized in this study complies with SNI 2049:2015 standards and was sourced from Semen Indonesia; the composition is presented in Table 1.

**Table 1. OPC content (semen Indonesia)**

| Chemical Compound | |
|---|---|
| $SiO_2$ % | 18.48 |
| $Al_2O_3$ % | 5.39 |
| $Fe_2O_3$ % | 3.23 |
| CaO % | 64.37 |
| MgO % | 2.16 |
| $SO_3$ % | 2.10 |
| LOI % | 3.80 |
| F-CaO % | 1.78 |

*3.1.2. Geopolymer Binder*

The geopolymer mortar utilized in this research was formulated using fly ash sourced from the Tanjung Jati B Power Plant in Jepara, Indonesia, serving as the primary aluminosilicate precursor. This material was combined with an alkaline activator, fine aggregates, and water. Chemical analysis revealed that the fly ash contains 83.87% combined $SiO_2$, $Al_2O_3$, and $Fe_2O_3$, thereby fulfilling the requirements for Class F fly ash as defined by ASTM C618, and confirming its suitability as a pozzolanic component in geopolymer systems. The fly ash exhibited a particle size below 0.075 mm (passing sieve No. 200) and contained no moisture. Detailed chemical composition is provided in Table 2, while surface morphology was examined via Scanning Electron Microscopy (SEM) at 2000× magnification, as presented in Figure 2.

**Table 2. Fly ash test results (test results)**

| Chemical Compound % | |
|---|---|
| $SiO_2$ | 46.52 |
| $Al_2O_3$ | 24.95 |
| $Fe_2O_3$ | 12.4 |
| CaO | 6.86 |
| MgO | 0.724 |
| $K_2O$ | 1.83 |
| $Na_2O$ | 1,59 |
| MnO | 0.06 |
| $TiO_2$ | 0.967 |
| $P_2O_5$ | 0.351 |
| LOI | - |

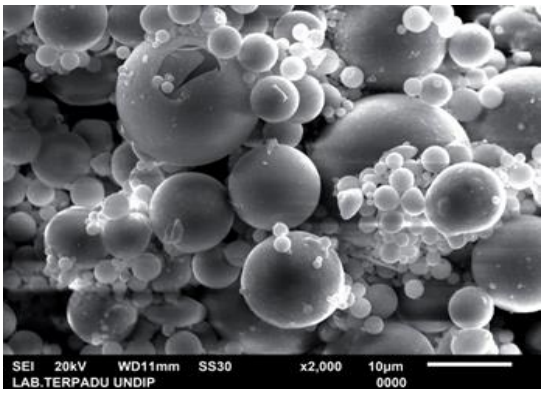


**Fig. 2 Scanning Electron Microscope (SEM) Fly Ash (source: Author Documentation)**

The precursors or activators employed to initiate the polymerization reaction consist of granular Sodium Hydroxide (NaOH) and Sodium Silicate Pentahydrate

($Na_2SiO_3.5H_2O$), as adopted in previous studies [14-17]. In this study, 14 Molar geopolymer was used because mortar will be used on structures that are submerged in water. The procedure for calculating and converting geopolymer binders is presented in Figure 3. Binder Geopolymer Calculation Procedure. In the calculation of geopolymer binders, the ratio of $SiO_2/Al_2O_3$ and $Na_2O/SiO_3$, greatly determines the strength of the geopolymer.

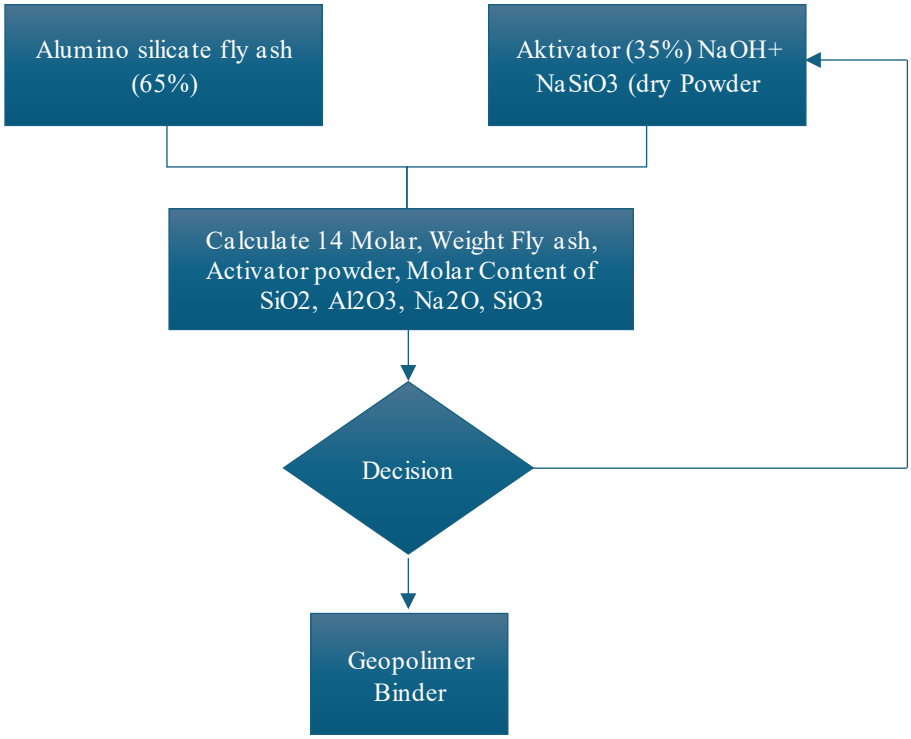


**Fig. 3 Dry geopolymer binder calculation procedure (own source)**

**Table 3. Compressive strength and activator ratio of geopolymer mortar mixes (test results)**

| Code | Activator Ratio | Component Ratio | | Compressive Strength MPa | Weight Volume kg/m³ |
|---|---|---|---|---|---|
| | | ($SiO_2$ /$Al_2O_3$) | ($Na_2O/SiO_3$) | | |
| MN 1 | - | | | 28,45 | 2,12 |
| MG1 | 1 : 2 | 4,49 | 0,32 | 27,49 | 2,10 |
| MG2 | 1 : 2,5 | 4,58 | 0,31 | 47,61 | 2,30 |
| MG3 | 1 : 3 | 4,65 | 0,31 | 30,41 | 2,26 |
| MG4 | 1 : 1,25 | 3,44 | 0,21 | 67,56 | 2,32 |

Based on the data presented in Table 3, the geopolymer mortar with an activator ratio of 1:2.5 (MG2) exhibited higher compressive strength compared to the MG1 and MG3 mixtures. This result indicates that the selected activator ratio contributes to a more optimal geopolymer matrix formation.

Therefore, the MG2 mixture was selected for further testing, including the underwater abrasion and sorptivity tests, alongside the Normal Mortar (MN) as a comparative reference.

*3.1.3. Fine Aggregates*

The fine aggregates utilized in this investigation were sourced from Muntilan, Central Java, and demonstrated a well-graded particle distribution, as presented in Figure 4. These aggregates are composed of natural sand, which may originate from riverbeds, quarries, or crushing processes, and may also include a combination of both sources. According to standard classification, fine aggregates are materials with a particle size less than 4.8 mm. Particles smaller than 1.2 mm are considered fine sand; those below 0.075 mm are classified as silt; and particles finer than 0.002 mm are called clay.

In contrast to ASTM C33, which classifies fine aggregates strictly as either natural or manufactured, the aggregates used in this study include both types. The fine aggregate passed the 4.75 mm sieve, exhibited a sludge content of 0.2%, and had an organic content characterized by a light-yellow color. The fineness modulus ranged between 2.3 and 3.1. The measured specific gravity of the material was 1.684 t/m³, while its moisture content was determined to be 0%.

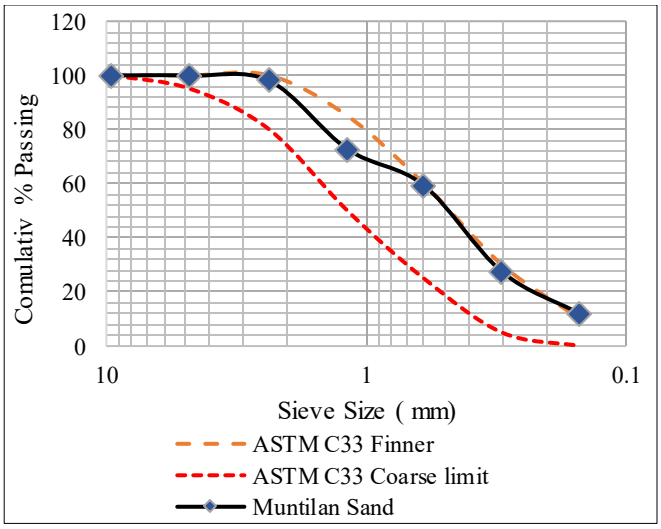


**Fig. 4 Analysis of muntilan sand (source: author documentation)**

### *3.2. Mortar Mix Proportion*

Referring to the requirements outlined in ASTM C270 for masonry mortars intended for outdoor exposure and submerged conditions, this study utilizes a binder-to-aggregate ratio of 1:2 as the base mixture. This ratio is selected to ensure adequate durability and workability under aggressive environmental conditions. The mix composition for producing 1 $m^3$ of mortar is presented in Table 4.

**Table 4. Mortar composition**

| Material | Combination | |
|---|---|---|
| | MN | MG |
| Portland Cement ($kg.m^{-3}$) | 800 | |
| Fly Ash ($kg.m^{-3}$) | | 520 |
| NaOH ($kg.m^{-3}$) | | 34 |
| $NaSiO_3$ Pentahidrat ($kg.m^{-3}$) | | 187 |
| Sand ($kg.m^{-3}$) | 1600 | 1600 |
| Water ($kg.m^{-3}$) | 424 | 192 |

Based on the mortar mix design presented in Table 4, MN represents the Ordinary Portland Cement (OPC) mortar, while MG is designated as the geopolymer mortar mixture. Both mortar types are prepared using a binder-to-fine aggregate ratio of 1:2 by weight. Initially, the binder and fine aggregate are dry mixed in a mechanical mixer for 5 minutes to ensure homogeneous blending. After the dry mixing stage, water was introduced based on the specified water-to-binder (w/b) ratios of 0.53 for MN and 0.26 for MG. Mixing continued for 4 minutes to ensure a homogeneous and consistent mortar blend. The flow table apparatus was employed to examine the workability of the fresh mortar mix, according to ASTM C1437, to evaluate the flow behavior of each mortar composition.

### *3.3. Experimental Investigation*

This study aims to evaluate the durability performance of geopolymer mortar against surface abrasion and erosion in hydraulic structures. A comprehensive experimental program was conducted, including compressive strength testing, underwater abrasion testing, and sorptivity testing, to assess mechanical properties and long-term durability. Additionally, to examine surface changes resulting from abrasion, an image processing approach was applied using Python in combination with the OpenCV library.

#### *3.3.1. Compressive Strength*

The compressive strength of hydraulic cement mortars was determined in accordance with ASTM C109 standard procedure, and was evaluated using the standard test method. For each mix variation, nine cube specimens measuring 50 mm × 50 mm × 50 mm were cast. The test was conducted by applying an axial load that increased continuously until the specimen reached failure. Compressive Strength was determined by dividing the maximum applied load (P) by the specimen's cross-sectional area (A), as defined in Equation (1). The test was conducted using a Jinan universal testing machine with a maximum load capacity of 300 kN, as illustrated in Figure 5.

$$\text{Compresive Strenght} = \frac{P}{A} \quad (1)$$

**Fig. 5 Compression testing machine (source: author documentation)**

#### *3.3.2. Underwater Abrasion Test*

In accordance with ASTM C1138, the abrasion resistance of mortar specimens was tested under submerged conditions using cylindrical samples sized 300 mm in diameter and 50 mm thick. Each specimen was positioned within a rotating steel drum containing water and a standardized abrasive charge consisting of steel balls: 10 with a diameter of 1 inch, 35 of 0.75 inch, and 25 of 0.5 inch. This configuration was employed to simulate hydraulic abrasion conditions and evaluate material degradation under dynamic impact and frictional forces.

The test apparatus was operated at a rotational speed of 1200 rpm for 72 hours. Measurements were taken at 12-hour intervals, during which each specimen was removed, cleaned, photographed, and weighed to determine material loss. The underwater abrasion test setup is illustrated in Figure 6. The

evaluation of abrasion resistance was performed using Equations (2) through (6), which are presented below [18, 19].

$$\mathrm{Vt} = \frac{\mathrm{Wair} - \mathrm{W\ water}}{Gw} \quad (2)$$

$$V\ lt = "Vi' - Vt \quad (3)$$

$$\mathrm{A\ D\ At'} = "\mathrm{VLt} / \mathrm{A} \quad (4)$$

$$PAWL\,(\%) = 100 * (\mathrm{wo} - \mathrm{wt})/\mathrm{wo} \quad (5)$$

$$IPA(\%) = 100 * (VAMN - VAGM)/VAMN \quad (6)$$

His research utilized multiple analytical indicators to assess the abrasion resistance of mortar specimens. The total volume of each specimen is represented by $V_t$, while $V_{lt}$ denotes the volume of material removed during a single abrasion cycle. The Abrasion Depth per cycle ($ADA_t$) is calculated by dividing the volume loss by the specimen's cross-sectional area (A). To evaluate the extent of mass reduction, the Percentage of Abrasion Weight Loss (PAWL) is determined based on the initial mass ($w_0$) and the remaining mass ($w_t$) following each testing interval. The Index of Abrasion Resistance Improvement (IPA) is introduced to assess the relative enhancement in durability among different mortar formulations. Additionally, VA denotes the cumulative abrasion volume at the end of testing. These parameters underpin the computational framework for assessing surface degradation and abrasion resistance, as outlined in Equations (2) through (6).

**Fig. 6 ASTM C1138 underwater abrasion test apparatus (source: author documentation)**

*3.3.3. Sorptivity Test*

The sorptivity evaluation was conducted based on the guidelines outlined in ASTM C1585, which specifies the procedure for assessing the rate of water uptake in hydraulic cement-based concrete. This test quantifies water absorption by monitoring the mass gain of a sample over time, caused by capillary action, with the condition that water contacts only one face of the specimen. In the present research, the test utilized a tubular Ø 100 mm and 50 mm in thickness. For each mortar mixture type, two specimens were prepared to ensure the reliability of the results [20].

### *3.4. Image Processing*

The image processing workflow in this study is developed to calculate the cross-sectional area of the specimen through a structured sequence of digital image analysis techniques. The process begins by importing the original image and converting it into a grayscale format to eliminate redundant color information and simplify data processing. Subsequently, the image is cropped and resized to ensure dimensional consistency and to focus on the region of interest [21].

A masking operation is then applied by inserting the image into a circular frame to isolate the object from its background and reduce edge noise. Following this, thresholding is performed to separate the object from the background based on pixel intensity values. To further enhance the quality of the binary image, a series of morphological filtering operations—such as Gaussian blur, erosion, and dilation—are applied to refine the object boundaries.

The enhanced image is then subjected to edge detection and contour extraction to accurately define the object's perimeter. Finally, the cross-sectional area is computed based on the detected contours, enabling quantitative analysis of surface geometry.

## 4. Results and Discussion

The results for Ordinary Portland Cement-based mortar (MN) and Geopolymer Mortar (GM) are analyzed and presented through a series of graphs and tables. The discussion includes a comprehensive analysis of abrasion depth, weight loss due to abrasion, the effect of mortar age on abrasion resistance, and sorptivity performance. These findings are critically compared with previous studies to highlight similarities, differences, and potential improvements the geopolymer mortar system offers.

### *4.1. Influence of Mortar Age on Abrasion*

Figure 7 presents the correlation between Abrasion Depth (ADA) and testing duration, with DA plotted on the y-axis and time on the x-axis, for both MN (Ordinary Portland Cement mortar) and MG (Geopolymer Mortar). At 3 days, both mortar types exhibit notably greater ADA values compared to those at 28 days. This trend aligns with expected material performance, as resistance to surface wear improves over time, attributable to continued cement hydration in OPC and the advancement of geopolymerization in geopolymer systems.

OPC-based and geopolymer mortars exhibit increased compressive strength over time, directly contributing to their enhanced abrasion resistance. Another notable observation is that improved mortar quality with age results in a more

pronounced difference in ADA between early and later ages. For the MN sample, ADA values were recorded at 8.7 mm at 3 days and reduced to 2.1 mm at 28 days. In the case of the geopolymer mortar (MG), ADA values were significantly lower, measuring 7.15 mm at 3 days and decreasing to only 0.14 mm at 28 days.

These findings are consistent with the results reported by Abid et al., which demonstrated that abrasion depth decreases proportionally with increased curing age and improved concrete quality.

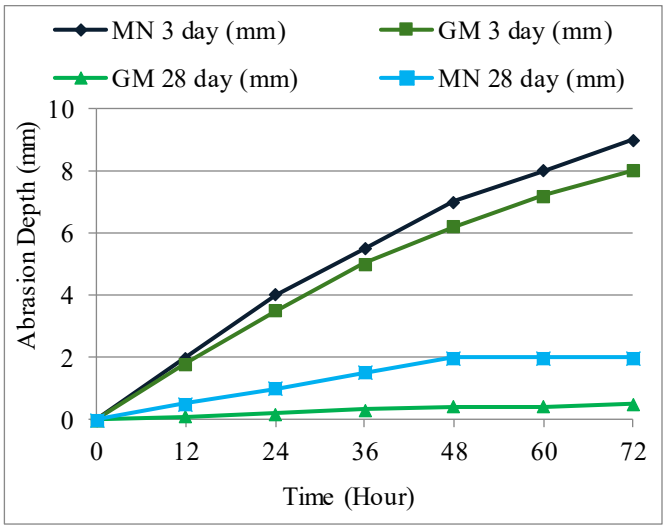


**Fig. 7 Depth of abrasion (source: author documentation)**

### *4.2. Comparison between MN and GM*

This section presents a comparative analysis between geopolymer mortar (MG) and conventional mortar (MN), both prepared with an identical mix ratio of 1 part binder to 2 parts aggregate. The comparison focuses on compressive strength, PAWL, surface changes and damage patterns observed under identical testing ages.

**Table 5. Mortar compressive strength 1:2**

| Sample | Compressive Strength 3 Days | Compressive Strength 28 Days |
|---|---|---|
| MN | 3.5 | 28,7 |
| MG 2 | 15.7 | 47,64 |

The compressive strength test results, as presented in Table 5, indicate that MG recorded a compressive strength of 47.64 MPa, while MN reached 28.7 MPa. Both mixtures were designed with the same binder-to-aggregate ratio of 1:2. These results demonstrate that geopolymer mortar exhibits significantly higher compressive strength than conventional mortar under identical mix proportions. The improved mechanical performance is primarily attributed to the geopolymerization mechanism, which facilitates the formation of robust chemical bonds between the binder matrix and aggregates. The optimized mixture proportions—particularly the sodium-to-silicate (Na/Si) ratio and the water-to-binder (w/b) ratio—play a pivotal role in achieving early-age strength development. These findings are consistent with prior research, which also demonstrated that geopolymer concrete generally attains higher compressive strength than conventional Portland cement-based systems under comparable conditions. Consequently, the superior mechanical characteristics of geopolymer mortar reinforce its viability as a sustainable and high-performance alternative for structural and durability-critical applications [22].

The comparison between conventional mortar (MN) and geopolymer mortar (MG) regarding abrasion resistance was evaluated based on weight loss after abrasion testing for 72 hours, with measurements taken at 12-hour intervals. The results, presented in Figure 8, are expressed as the percentage of weight loss calculated from the specimen's mass before and after testing. At the age of 3 days, the MN specimen experienced a weight loss of 13.68%, while the MG specimen exhibited a lower weight loss of 11.34%. MG's weight loss reduction is attributed to its enhanced compressive capacity, resulting in improved wear and particle collision resilience during abrasion assessment.

At 28 days, the difference becomes more significant. The MN specimen recorded a Percentage of Accumulated Weight Loss (PAWL) of 3.38%, whereas the MG specimen showed a minimal loss of only 0.31%. This superior performance of geopolymer mortar is due to the continued polymerization reaction, which leads to a denser and more cohesive matrix. MG's enhanced mechanical properties, particularly compressive strength, provide greater resistance to abrasion, validating its potential application in structures exposed to an aggressive hydraulic environment. These results align with previous research, where wet geopolymer concrete has a better PAWL value than conventional concrete.

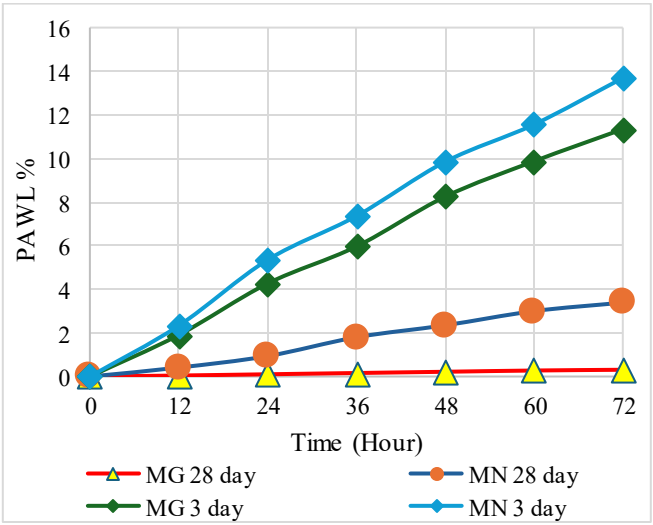


**Fig. 8 Percentage Abrasion of Weight Loss (PAWL) (source: author documentation)**

In addition to weight loss, the abrasion test results based on ASTM C1138 were also expressed in terms of volume loss over a total testing duration of 72 hours. For conventional mortar (MN), the abrasion volume loss at the age of 3 days was recorded at $4.95 \times 10^{-4}$ m³; at 28 days, it decreased to $3.75 \times 10^{-4}$ m³. In comparison, geopolymer mortar (MG) exhibited significantly lower abrasion volume loss values of $1.44 \times 10^{-4}$ m³ at 3 days and $7.68 \times 10^{-6}$ m³ at 28 days, as shown in Figure 9.

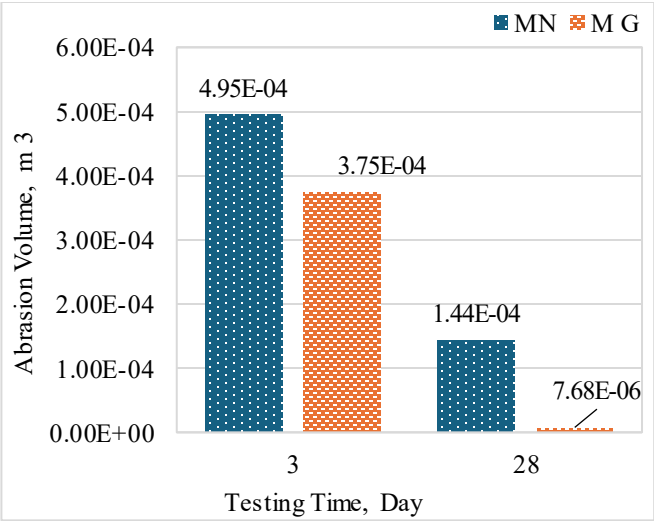


**Fig. 9 Comparison of abrasion volume loss between conventional and geopolymer mortar over curing time. (source: author documentation)**

The improvement in abrasion resistance is further quantified using the Abrasion Resistance Improvement Index (IPA), calculated using Equation (6), which compares the volume loss between geopolymer and conventional mortar at each testing age. At 3 days, the IPA value between MN and MG was 24.29%, while at 28 days, the IPA value increased significantly to 92.87%, indicating a substantial enhancement in resistance as the geopolymer matured.

Additionally, the abrasion resistance development ratio was evaluated by comparing the abrasion volume loss of each mortar type between 3-day and 28-day curing ages. For MN, the reduction ratio was approximately 3.45 times, while for MG, the improvement was much more significant, reaching 36.58 times. These results clearly demonstrate the superior long-term abrasion resistance of geopolymer mortar compared to conventional mortar under identical testing conditions.

The surface damage patterns of both Conventional Mortar (MN) and Geopolymer Mortar (MG) can be observed in Figure 10. The damage resulted from the continuous friction between steel balls and the mortar surface during the ASTM C1138 abrasion testing. In mortars with lower compressive strength, the damage was characterized by forming localized pits with relatively large diameters. This phenomenon occurs due to the erosive action of steel balls grinding the surface and initiating cavitation-like surface cracking. Notably, the surface degradation was concentrated outside the radius covered by the lower section of the rotating paddle, indicating that steel balls were displaced radially outward due to centrifugal forces. This pattern is aligned with previous findings reported by Abdulhasan et al. [23-25] who reported comparable surface degradation patterns in both Ordinary Portland Cement (OPC) concrete and geopolymer concrete subjected to identical abrasion conditions. The resemblance in wear characteristics indicates that the mechanical strength of the mortar and the dynamic motion of abrasive particles within the testing environment predominantly governs abrasion-induced damage.

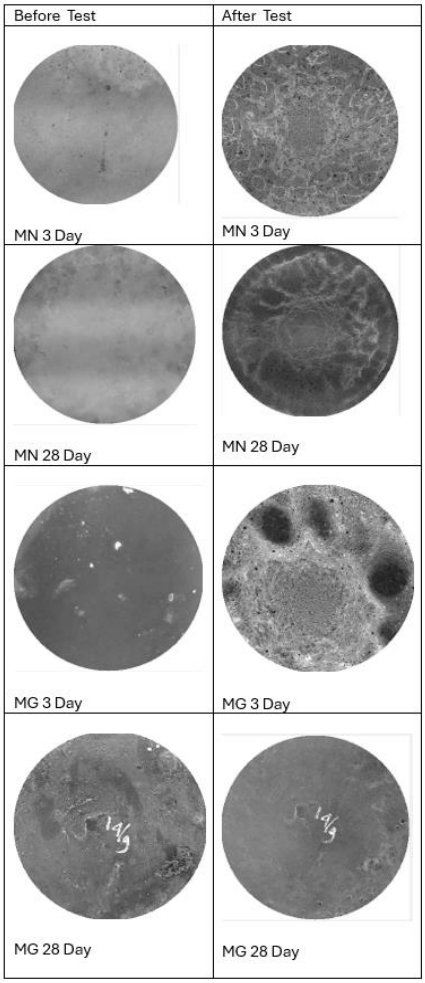


**Fig. 10 Sample photos test before and after the abrasion test. (source: author documentation)**

### *4.3. Image Processing and Validation*

Applying digital image processing techniques in calculating abrasion volumes provides a non-destructive, efficient, and replicable approach to material degradation analysis. In this study, two-dimensional images of the surface of mortar specimens undergoing underwater abrasion testing were processed using Thony Python and the OpenCV library

to estimate the volume of material loss. The image analysis process is carried out through several stages: conversion to grayscale, image segmentation using thresholding techniques, morphological screening (Gaussian blur, erosion, and dilation), and contour detection to isolate abrasion areas. The area of abrasion obtained in pixels is then converted to physical units (mm²) using a calibration scale obtained from the reference object in the image. The estimated abrasion volume is then calculated by multiplying the abrasion area by the average abrasion depth, which is determined experimentally or based on the surface profile.

The image processing results can be seen in Figure 11, which shows the filtration and segmentation of 2-dimensional images of abrasion test results. The part that forms the hole due to the impact of the steel ball is stated as the part that has a hole shown on the elevation map. The volume of abrasion is then calculated from the area of the lost cross-section.

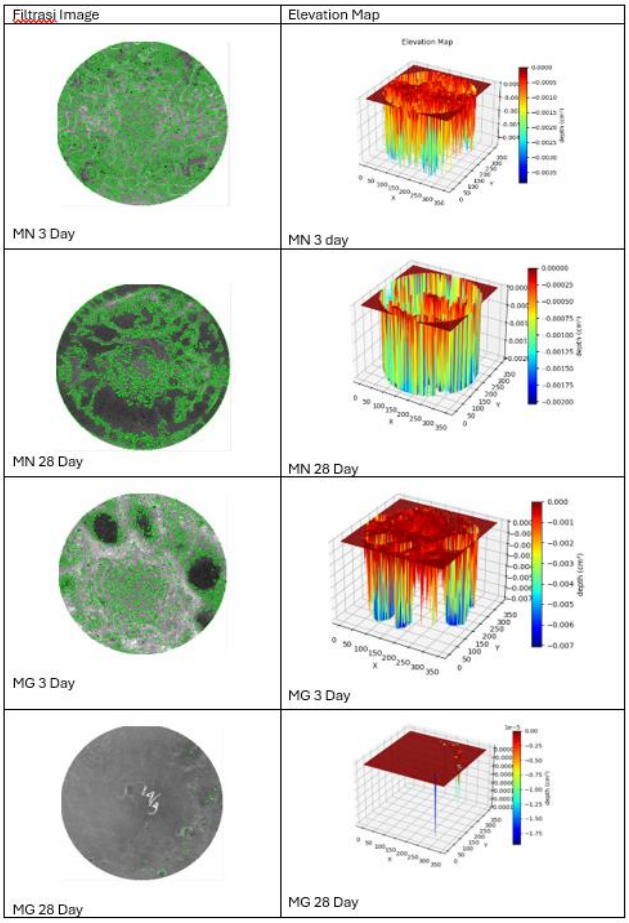


**Fig. 11 Image processing, filtration and elevation map. (source: author documentation)**

Validation of the image processing analysis was performed by comparing the results with the actual weight measurements of the specimens. The outcomes are presented in Table 6. For samples exhibiting significant surface degradation, the image-based analysis yielded relatively low error rates of 2.84%, 5.15%, and 3.71%, respectively. However, in specimens where abrasion occurred uniformly without the formation of visible pits or cracks, the accuracy of the image analysis decreased substantially, with an error rate reaching 24.95%.

**Table 6. Validation of image processing**

| Sample Code | Abrasion by weight | Abrasion by Image | Err % |
|---|---|---|---|
| MN 3 | 4,95E-04 | 5,09E-04 | 2,84 |
| MG 3 | 3,75E-04 | 3,94E-04 | 5,15 |
| MN 28 | 1,44E-04 | 1,49E-04 | 3,71 |
| MG 28 | 7,68E-06 | 9,60E-06 | 24,95 |

### *4.4. Effect of Sorptivity on Abrasion*

Figure 12 shows the relationship between sorpivity (I) and the time root (√t) for two types of specimens, namely MG and MN. Sorption is an essential parameter in evaluating the ability of porous materials, such as mortar or concrete, to absorb water through capillaries. The higher the sorptivity value, the greater the potential for water to enter the material's pores, which in the long term can affect the structure's resistance to damage due to moisture or aggressive ions. These findings have the same pattern as previous research [26, 27].

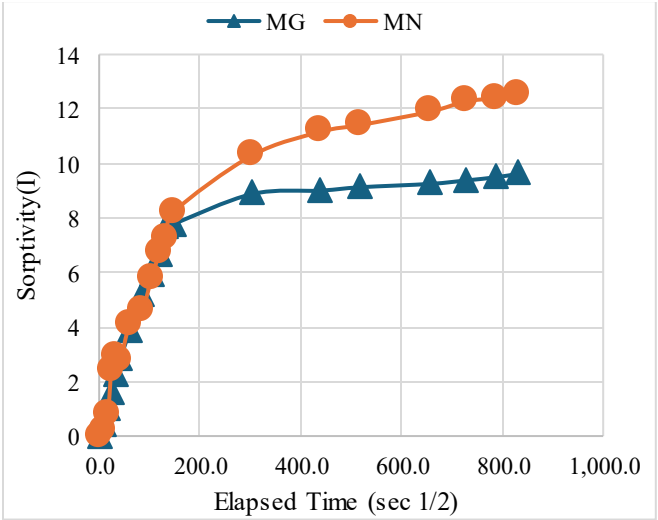


**Fig. 12 Graphic sorptivity (source: author documentation)**

Based on the graph, it can be seen that MN specimens show higher sorpivity values than MG over the entire test time range. The increase in sorpivity in MN is very sharp at the beginning, indicating that the material's microstructure has a high open porosity and capillary pathways that allow water to be absorbed quickly. In contrast, MG specimens show a slower increase in sorpivity and reach a stable state after a specific time, indicating the presence of a tighter pore structure or the influence of additives that inhibit water absorption. This difference in sorpivity pattern has important implications for material resistance. The high sorpivity value

in MN indicates that the material is more susceptible to degradation due to the penetration of water and aggressive substances from the environment, such as chloride or sulfate ions. Meanwhile, an MG that shows a lower sorpivity value is considered more resistant to water absorption. It is more suitable for use in environments with high humidity levels or continuous water exposure, such as construction in coastal areas or underground structures.

## 5. Conclusion

This study experimentally demonstrated that geopolymer mortar (MG) performs significantly better than conventional Ordinary Portland Cement mortar (MN) regarding underwater abrasion resistance, making it a promising alternative for hydraulic structures exposed to aggressive flow conditions. At 28 days of curing, MG recorded an abrasion volume loss of only $7.68 \times 10^{-6}$ m³, while MN experienced a loss of $3.75 \times 10^{-4}$ m³, indicating that MG has approximately 48.83 times greater abrasion resistance. At 3 days, MG outperformed MN with a resistance ratio of 3.44. The Abrasion Resistance Improvement Index (IPA) increased from 24.29% at 3 days to 92.87% at 28 days, and the reduction in abrasion volume from 3 to 28 days was 36.58 times for MG, compared to only 3.45 times for MN. These results confirm the superior long-term durability of the geopolymer system.

In addition to abrasion resistance, MG demonstrated enhanced mechanical and durability properties. It achieved a compressive strength of 47.64 MPa at 28 days, significantly higher than MN's 28.7 MPa. The sorptivity test results showed that MG had a lower water absorption rate, indicating a denser microstructure and better resistance to moisture and aggressive ions. These characteristics make geopolymer mortar more suitable for high-humidity or submerged environments. Furthermore, using fly ash as the primary binder contributes to a lower carbon footprint, positioning geopolymer mortar as a more sustainable and environmentally friendly alternative to OPC-based systems.

For future research, it is recommended to investigate the chemical resistance of geopolymer mortar against sulfate and chloride attacks, conduct advanced microstructural analyses using XRD, FTIR, and SEM, and explore incorporating natural or synthetic fibers to enhance crack resistance.

## Acknowledgments

Appreciation is extended to the Doctoral Program in Civil Engineering at Sultan Agung Islamic University, Semarang, and the Jurusan Teknik Sipil Politeknik Negeri Semarang for the academic and technical support provided throughout this research.

## References

[1] Nicholas Omoding, Lee Cunningham, and Gregory F Lane-Serff, "Review of Concrete Resistance to Abrasion by Waterborne Solids," *Materials Journal*, vol. 117, no. 3, pp. 41-52, 2020. [CrossRef] [Google Scholar] [Publisher Link]

[2] Andrej Kryžanowski et al., "Abrasion Resistance of Concrete in Hydraulic Structures," *ACI Materials Journal*, vol. 106, no. 4, pp. 349-356, 2009. [CrossRef] [Google Scholar] [Publisher Link]

[3] Jinjun Guo et al., "Mechanisms and Influential Variables on the Abrasion Resistance Hydraulic Concrete," *Nanotechnology Reviews*, 2022. [CrossRef] [Google Scholar] [Publisher Link]

[4] Rawaa H. Ismaeil, Ali N. Hilo, and Thaar S. Al-Gasham, "Review of Abrasion Mechanisms and Influential Variables on The Disintegration Resistance of Concrete," *IOP Conference Series: Materials Science and Engineering*, Erbil, Iraq, vol. 1058, no. 1, pp. 1-10, 2021. [CrossRef] [Google Scholar] [Publisher Link]

[5] ACI 207.6R : 2017, Report on the Erosion of Concrete in Hydraulic Structures, American Concrete Institute, 2017. [Online]. Available: https://www.concrete.org/Portals/0/Files/PDF/Previews/207.6R-17_preview.pdf

[6] Yu-Wen Liu, Tsong Yen, and Tsao-Hua Hsu, "Abrasion Erosion of Concrete by Water-Borne Sand," *Cement and Concrete Research*, vol. 36, no. 10, pp. 1814-1820, 2006. [CrossRef] [Google Scholar] [Publisher Link]

[7] Jingfu Kang, Bo Zhang, and Guangyu Li, "The Abrasion-Resistance Investigation of Rubberized Concrete," *Journal of Wuhan University of Technology- Materials Science Edition,* vol. 27, no. 6, pp. 1144-1148, 2012. [CrossRef] [Google Scholar] [Publisher Link]

[8] Osamu Akashi et al., "A Projection for Global $CO_2$ Emissions from the Industrial Sector through 2030 based on Activity Level and Technology Changes," *Energy*, vol. 36, no. 4, pp. 1855-1867, 2011. [CrossRef] [Google Scholar] [Publisher Link]

[9] Angel Palomo, M.W. Grutzeck, and M.T. Blanco, "Alkali-Activated Fly Ashes: A Cement for the Future," *Cement and Concrete Research*, vol. 29, no. 8, pp. 1323-1329, 1999. [CrossRef] [Google Scholar] [Publisher Link]

[10] Ismail Luhar, and Salmabanu Luhar, "A Comprehensive Review on Fly Ash-Based Geopolymer," *Journal of Composites Science*, vol. 6, no. 8, pp. 1-59, 2022. [CrossRef] [Google Scholar] [Publisher Link]

[11] Ge Zhang et al., "Novel Selection of Environment-Friendly Cementitious Materials for Winter Construction: Alkali-Activated Slag/Portland Cement," *Journal of Cleaner Production*, vol. 258, 2020. [CrossRef] [Google Scholar] [Publisher Link]

[12] Joseph Davidovits, "Geopolymers and Geopolymeric Materials," *Journal of Thermal Analysis*, vol. 35, no. 2, pp. 429-441, 1989. [CrossRef] [Google Scholar] [Publisher Link]

[13] Tero Luukkonen et al., "One-Part Alkali-Activated Materials: A Review," *Cement and Concrete Research*, vol. 103, pp. 21-34, 2018. [CrossRef] [Google Scholar] [Publisher Link]

[14] M. Elzeadani, D.V. Bompa, and A.Y. Elghazouli, "One Part Alkali Activated Materials: A State-of-the-Art Review," *Journal of Building Engineering*, vol. 57, 2022. [CrossRef] [Google Scholar] [Publisher Link]

[15] Dhruv Sood, and Khandaker M.A. Hossain, "Fresh State, Rheological and Microstructural Characteristics of Alkali-Activated Mortars Developed using Novel Dry Mixing Technique Under Ambient Conditions," *Applied Sciences*, vol. 11, no. 19, pp. 8920-8920, 2021. [CrossRef] [Google Scholar] [Publisher Link]

[16] Ridho Bayuaji et al., "A Review in Geopolymer Binder with Dry Mixing Method (Geopolymer Cement)," *AIP Conference Proceedings*, vol. 1887, no. 1, pp. 1-6, 2017. [CrossRef] [Google Scholar] [Publisher Link]

[17] Himawan Tri Bayu Murti Petrus et al., "Green Geopolymer Cement with Dry Activator from Geothermal Sludge and Sodium Hydroxide," *Journal of Cleaner Production*, vol. 293, 2021. [CrossRef] [Google Scholar] [Publisher Link]

[18] Elzbieta Horszczaruk, and Piotr Brzozowski, "Effects of Fluidal Fly Ash on Abrasion Resistance of Underwater Repair Concrete," *Wear*, vol. 376-377, pp. 15-21, 2017. [CrossRef] [Google Scholar] [Publisher Link]

[19] Warun Wongprachum et al., "Resistance to Sulfate Attack and Underwater Abrasion of Fiber Reinforced Cement Mortar," *Construction and Building Materials*, vol. 189, pp. 686-694, 2018. [CrossRef] [Google Scholar] [Publisher Link]

[20] Shahir Ahmad Safi, and Khaled Waleed Radman, "Durability and Performance of Geopolymer Concrete: Sorptivity and Acid Attack Resistance," *6th International Conference on Applied Engineering and Natural Sciences*, Konya, Turkey, pp. 1-6, 2024. [Google Scholar]

[21] Mojtaba Kamani, and Rassoul Ajalloeian, "Investigation of the Changes in Aggregate Morphology during Different Aggregate Abrasion/Degradation Tests using Image Analysis," *Construction and Building Materials*, vol. 314, 2022. [CrossRef] [Google Scholar] [Publisher Link]

[22] Sallal R. Abid, Ali N. Hilo, and Yasir H. Daek, "Experimental Tests on the Underwater Abrasion of Engineered Cementitious Composites," *Construction and Building Materials*, vol. 171, pp. 779-792, 2018. [CrossRef] [Google Scholar] [Publisher Link]

[23] Kolli Ramujee, and M. Potharaju, "Abrasion Resistance of Geopolymer Composites," *Procedia Materials Science*, vol. 6, pp. 1961-1966, 2014. [CrossRef] [Google Scholar] [Publisher Link]

[24] Shams M. Cheyad, Ali N. Hilo, and Thaar S. Al-Gasham, "Comparing the Abrasion Resistance of Conventional Concrete and Geopolymer Samples," *Materials Today: Proceedings*, vol. 56, pp. 1832-1839, 2022. [CrossRef] [Google Scholar] [Publisher Link]

[25] Noor A. Abdulhassan et al., "Underwater Surface Abrasion of Conventional and Geopolymer Concrete using the ASTM C1138 Approach," *Journal of Materials Research and Technology*, vol. 25, pp. 2556-2569, 2023. [CrossRef] [Google Scholar] [Publisher Link]

[26] Ghasan Fahim Huseien et al., "Effective Microorganism Solution-Imbued Sustainable Self-Curing Concrete: Evaluation of Sorptivity, Drying Shrinkage and Expansion," *Case Studies in Construction Materials*, vol. 20, 2024. [CrossRef] [Google Scholar] [Publisher Link]

[27] Delista Putri Deni, 'Ilma Alfianarrochmah, and Oktavia Kurnianingsih, "Chloride Penetration and Sorptivity of High-Quality Self-Compacting Concrete with Variations in Metakaolin Substitution," *Journal of Civil and Environmental Engineering*, vol. 8, no. 2, pp. 115-126, 2023. [Google Scholar] [Publisher Link]